Measuring Material Properties through Gradient Based NMR: Diffusion and Imaging

Åslund, Ingrid

2010

Measuring Material Properties through Gradient Based NMR: Diffusion and Imaging

Ingrid Åslund

LUND UNIVERSITY

Doctoral Thesis

The thesis will be publicly defended on Saturday 18th of September 2010, 10.15 in lecture hall B, Center for Chemistry and Chemical Engineering, Lund

The faculty opponent is Prof Dr. William S. Price,
Nanoscale Organisation and Dynamics Group,
University of Western Sydney, Australia

Doctoral Thesis

Physical Chemistry
Center for Chemistry and Chemical Engineering
Lund University
P.O. Box 124
SE-221 00 Lund
Sweden

Title page: An T_1-weighted MR-image of the authors breast. Figure courtesy of Markus Nilsson.

ISBN 978-91-7422-247-0
Printed by Mediatryck, Lund University, Lund

Measuring Material Properties through Gradient Based NMR: Diffusion and Imaging

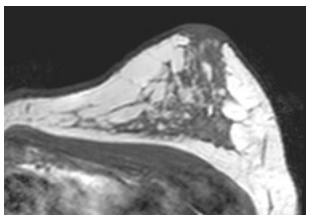

Organization
LUND UNIVERSITY

Physical Chemistry
Centre for Chemistry and Chemical Engineering
P.O.Box 124, SE-221 00 Lund, Sweden

Author(s)
Ingrid Åslund

Document name
DOCTORAL DISSERTATION

Date of issue
September 18, 2010

Sponsoring organization
SSF - Swedish Foundation for Strategic Research

Title and subtitle
Measuring Material Properties through Gradient Based NMR: Diffusion and Imaging

Abstract

In this work new methods based Nuclear Magnetic Resonance (NMR) have been developed to measure different kinds of structural properties in soft materials.

The advantage of using NMR as a technique to measure material properties is that it is non-destructive, which makes it possible to measure on the actual piece of material that will be used for the application. One does not have to be concerned with whether a small sample represents the whole material or if each piece is similar.

By applying a time-dependent gradient in the magnetic field the spins are labelled according to their position. This labelling can then be used either to make density images showing the local concentration or to monitor molecular displacements which carry information on sample structure. Both of these approaches have been used when developing the new NMR-methods, even if the focus has been on molecular displacement techniques.

The homogeneous length-scale is obtained by monitoring the displacement of the molecules on different length-scales. For small length-scales the microheterogeneous structures can be observed while for long length-scales an averaging is taking place and the sample will appear homogeneous. The homogeneous length-scale thus indicates the scale of the structural features in the system.

If different molecules can be followed independently further information of the structure can be obtained. One can identify obstacles and restrictions that effect a specific type of molecules. This can help to identify the structural features and what they are made up of. Existing experimental sequences were modified so that spectral resolution could be obtained.

For biological tissue the intracellular diffusion and cell wall permeability are interesting properties, not the least within the content of medical applications. Methods to measure these two properties have been developed and tried out on yeast cell suspensions.

Interbilayer forces were measured by centrifuging samples of lamellar phases with different concentration until equilibrium was reached. The concentration profile obtained at equilibrium and measured using magnetic resonance imaging was then used to obtain the bending rigidity.

All methods are based on previously established techniques but are here combined or used in new ways.

Key words: NMR, self-diffusion, lamellar phase, yeast suspensions, emulsions, material properties, homogeneous length-scale, intracellular diffusion, membrane permeability and bending rigidity

Classification system and/or index termes (if any):

Supplementary bibliographical information:

Language
English

ISSN and key title:

ISBN
978-91-7422-247-0

Recipient's notes

Number of pages
162

Price

Security classification

Preface

This thesis is a summary of my work during 4.5 years as a PhD-student at Physical Chemistry, Lund University. The aim of the project has been to develop new techniques and methods to measure material properties using Nuclear Magnetic Resonance (NMR) and molecular diffusion. Because of the accessibility and presence of water the molecular diffusion has been monitored for this molecule.

The main advantage of NMR as a measuring technique is that it is non-destructive, implying that the sample is the same before and after the measurement. Using a probe like water also makes the technique interesting for medical and biological application, since at least 60% of the weight of the biological tissue is water.[1] This is, for example, taken advantage of in Magnetic Resonance Imaging (MRI) preformed on living organisms.

The thesis has two parts; a summary, meant to be an introduction for the non-specialist, and a compilation of the research publications. The first part is organized to give a general overview of the research field. After a short introduction, the studied systems used are introduced before continuing with a short description of the phenomenon of diffusion. After that comes an overview of NMR and the developed methods before the conclusions finish this part.

List of Papers

This thesis is a summary of the following papers. They will be referred to by their Roman numbers throughout the text. The articles are included at the end of the thesis.

I **Diffusion NMR for Determining the Homogeneous Length-Scale in Lamellar Phases**
Ingrid Åslund, Celia Cabaleiro-Lago, Olle Söderman and Daniel Topgaard
Journal of Physical Chemistry B, **2008**, *112*, 2782-2794

II **Homogeneous Length Scale of Sheared-induced Multilamellar Vesicles Studied by Diffusion NMR**
Ingrid Åslund, Bruno Medronho, Olle Söderman, Daniel Topgaard and Claudia Schmidt
Manuscript, **2010**

III **Spectral Characterization of Diffusion with Chemical Shift Resolution: Highly Concentrated Water-in-Oil Emulsion**
Samo Lasič, Ingrid Åslund and Daniel Topgaard
Journal of Magnetic Resonance, **2009**, *199*, 166-172

IV **Investigations of Vesicle Gels by Pulsed and Modulated Gradient NMR Diffusion Techniques**
Samo Lasič, Ingrid Åslund, Claudia Oppel, Daniel Topgaard, Olle Söderman and Michael Gradzielski
Manuscript. **2010**

V **Determination of the Self-Diffusion Coefficient of Intracellular Water Using PGSE NMR with Variable Gradient Pulse Length**
Ingrid Åslund and Daniel Topgaard
Journal of Magnetic Resonance, **2009**, *201*, 250-254

VI **Filter-Exchange PGSE NMR Determination of Cell Membrane Permeability**
Ingrid Åslund, Agnieszka Nowacka, Markus Nilsson and Daniel Topgaard
Journal of Magnetic Resonance, **2009**, *200*, 291-294

VII **Lamellar Phase Separation in a Centrifugal Field. A Method for Measuring Interbilayer Forces**
Sanja Bulut, Ingrid Åslund, Daniel Topgaard, Ulf Olsson and Håkan Wennerström
Soft Matter, **2010**, *in press* (DOI:10.1039/C0SM00085J)

List of Contributions

I I did the main analysis of the results, both experiments and simulations, and was responsible for the writing.

II I took part in performing the experiments and carried out the analysis. I was responsible for the writing of the paper.

III I took part in setting up experiments and interpreting the results. I also contributed to the writing.

IV I was responsible for the PGSE-part of the project, both regarding experiments and writing.

V I performed the experiments, analyzed them and did parts of the writing.

VI I supervised the initial work, did the complementary experiments and analysis and was responsible for writing the paper.

VII I took part in performing the experiments, made the analysis and contributed to the writing.

Acknowledgements

I should start with thanking **Peter Mohlin** because without him telling me about the position announced on the Lund University homepage I would not known about this project at all.

Of course the next on the list is my supervisor **Daniel Topgaard**, both for having the courage to take me on as a PhD-student without knowing that much about me and for all the help during these 4.5 years.

Not to be forgotten is my assistant supervisor **Olle Söderman** who has, despite a busy schedule, never rejected to answer a question or discuss a problem.

I would also like to thank my different co-aurthors: **Celia Cabaleiro-Lago** for the preparation and experiments on the lamellar phases, **Bruno Medronho** and **Claudia Schmidt** for introducing me to the "onion"-phase, **Samo Lasič** for showing me the world of modulated gradients, **Claudia Oppel** and **Michael Gradzielski** for sending their vesicle gels to Lund, **Agnieszka Nowacka** and **Markus Nilsson** for a nice collaboration on exchange and **Sanja Bulut**, **Håkan Wennerström** and **Ulf Olsson** for letting me take part in the centrifugation project.

I would have gotten nowhere without the patience of **Carin Malmborg**, **Geraldine Lafitte** and **Markus Nilsson** answering all my initial questions about running an NMR-spectrometer. **Gabriel Rata**, **Samo Lasič**, **Christina Wende**, **Tiago Ferreira** and **Agnieszka Nowacka** are acknowledged for all discussion and help with the struggles of NMR-spectrometers and Matlab.

Without the knowledge and help from **Hans Lilja** and **Lennart Nilsson** fighting the errors in the spectrometers would have been nearly impossible. The administrative and chemical necessities have been made so much easier by **Majlis Larsson** and **Ingegerd Lind**.

I also enjoyed and learned something from all the people I help out doing NMR-experiments. Especially **Agnieszka Nowacka**, **Nagore Arteaga**, **Simon Küster**, **Mattias Björklund** and **Niklas Häggman** who's diploma or summer projects I took part in supervising.

Markus Nilsson and **Jimmy Lätt** are thanked for the (for me) invaluable discussions on imaging and introducing me to hospital MR-scanners. They also made the picture on the title page possible.

All of Physical Chemistry are acknowledged for the nice working atmosphere and especially fkem United and the badminton group. Also **Colloidal Resource** should be mentioned, including the enthusiasm of **Anna Stenstam** and **Karin Bryskhe** for the FEXSY-project.

I would never have survived without the possibility to play and travel with my orchestras **Alte Kamereren**, **Chalmers Barockensemble** and **Göteborgspolisens Musikkår**. Especial thanks go to **Leo** and **Staffan** for making up a great committee and helping me out when I could not fulfill my obligations because of the work presented in here. I would also like to thank **Maria** for all the chitchats on supervisors, instruments, reviewers and everything else regarding being a PhD-student.

For me great, relaxing times have been spent with **Bettan**, **Olle**, **Claes** and **Birgitta** in and out of Halmstad. I have always felt you support and hope I have been able to give some back.

I would not be where I am today without the love, care and support of **Mamma**, **Pappa**, **Erik** and **Ulrika** .

Last, but not least, comes **Johan**, who should be thanked for putting up with me and all the travels between Lund and Göteborg and also for helping me to keep in mind what is important.

Contents

Chapter 1

Introduction

Understanding material properties is crucial for the application of the material. Without knowing its properties it is impossible to know whether the material can handle the stress and/or strain it will be exposed to, or to know if the material transmits enough light. Of course, these are just two examples from a huge list of material properties which one needs to know to make an appropriate choice of a material for a particular application.

Everything around us is made up of materials, the air we breath could be considered a material, the chair we sit in is a "skeleton" of hard material with maybe some softening textile material, the metal surrounding the tanks in a chemical reaction plant is a material, but also hygiene products, such as toothpaste and shampoos. The latter examples belong to the class of soft materials.

In this work properties of soft materials have been measured through the development of new NMR methods. These new techniques have all used gradients in the magnetic field to label the molecules with respect to their spatial location. This label has then been used to measure molecular diffusion and/or images, i.e. maps of molecular position.

The properties measured were; 1) the homogeneous length scale, viz. the maximum length scale for microstructural heterogeneities in a macroscopically homogeneous material 2) the diffusion experienced by different components, which contains innformation about the different environments and structures that the different components can experience 3) the local self-diffusion coefficient in the intracellular space of living cells, which depends on the organization of, e.g.,the cytoskeleton and organelles 4) the rate of molecular exchange between extra- and intracellular space, which is related to the proprties and integrity of the cell membrane 5) concentration profiles of lyotropic lamellar liquid crystals equilibrated in

a strong gravitational field, from which the forces between surfactant bilayers can be calculated.

Chapter 2

Soft Materials

Soft materials, or soft matter, are things that deform and change shape under stress.[2] This includes gels, liquid crystals and biological materials but also suspensions and more liquid-like materials. In this work the focus has been on relatively viscous materials, where the three earlier categories form a major part.

Any material which is stiff but still possible to reshape with a reasonable amount of force could in a non-strict way be referred to as a gel. The strict definition is extended regions which are solid-like and in contact with extended regions which are liquid-like.[3] As examples one can mention polymer networks swelled with water or materials of a gel phase. The latter are lamellar materials with non-polar regions of solid phase while the water regions in between are in the liquid phase (very similar to a lamellar phase, see section 2.1 for a further description). The lamellar phase is an example of a soft material with liquid properties that is periodic in its structure. Such materials are known as liquid crystals. Often liquid crystals are made up of surface-active agents, also known as surfactants (see section 2.1). Polar lipids, the natural analogs of surfactants, are some of the compounds needed to make a biological cell (see section 2.2) and thus biological materials. From this discussion it is clear that although soft materials have very different origins and applications, they have many things in common.

Apart from being interesting from a fundamental point of view, to learn more about physics, chemistry and biology, soft materials have a wide range of applications.[2–5] Basically any hygiene product, such as cosmetics and soaps, is a soft material but they are also used in liquid crystal displays and in paints. They are also interesting in an industrial context as templates to create other materials with a certain shape and/or size[6] but also to create materials with high surface-to-volume ratios to obtain

the catalytic effect needed for chemical reactions.[7]

2.1 Surfactants

The characteristic feature of a surfactant is that it is amphiphilic, and as a consequence it is made up of two parts:[2–4] one part which is hydrophilic and thus likes to be in water and the other, known as the hydrophobic part, which dislikes water. The hydrophobic part, also called the surfactant tail, is generally one or two chains of hydrocarbons but can also contain hydrocarbon rings. The important property is its non-polarity and thus it avoids water. The hydrophilic part, also called the surfactant headgroup, is polar and thus interacts with water. Depending on the type of headgroup the surfactant can be anionic, cationic, zwitterionic or nonionic. For an anionic surfactant the headgroup is negatively charged, while the cationic surfactant has a cation as headgroup. A zwitterionic surfactant has both a positive and negative charge in its headgroup. In the case of nonionic surfactants there is no charge but the headgroup is polar through a directionality in the non-evenly distributed electron clouds. Two examples of nonionic surfactants have headgroups of glucose or oligomers of the water soluble polymer polyethylene-glycol. A basically endless list of different surfactants can be made by combining different heads and tails. Some examples can be found in Figure 2.1.

It is the surfactants amphiphilicity that makes it enrich at interfaces between areas of polar substances (such as water) and non-polar substances (such as oil or air). The headgroup orients towards the polar environment while the tail gathers in the non-polar regions. It is this property that makes surfactants self-assemble and form different structures. A self-assembled structure is homogeneous on the macroscopic scale (visible by eye) but on the microscopic scale (μm and nm) structural features are noticeable. This phenomenon is illustrated in Figure 2.2.

This concept of a sample appearing homogeneous on one length-scale but not on another length-scale is used to define the homogeneous length-scale, λ_{hom}. The length for the transition between the microscopic scale, where structural heterogeneities appear, and the microscopic scale, where material appears homogeneous, is λ_{hom}. One could think of λ_{hom} as the pixel size for which a picture loses its details. Starting from a detailed picture with high resolution and adding together the pixels two and two the picture will after a certain amount of pixel additions appear completely uniform, compare Figure 2.3. The size of the pixel when the

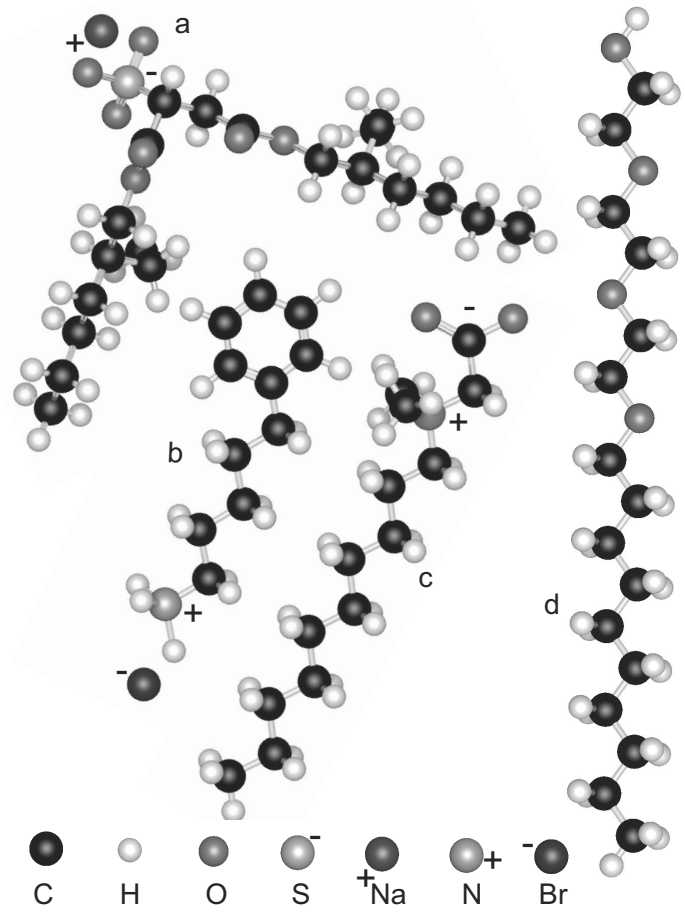

Figure 2.1: Illustrations of examples of different type of surfactants, anionic (a), cationic (b), zwitterionic (c) and nonionic (d). For the mono-ionic surfactants (b and c) a counterion (which is needed to obtain charge neutrality) is also included. The different type of atoms are indicated at the bottom of the figure. Note that the anionic charge for the zwitterionic surfactant is a carboxylate making it an amino acid derivative. The anionic surfactant is Aerosol OT used in paper I and the nonionic surfactant is $C_{10}E_3$, used in papers II and VII

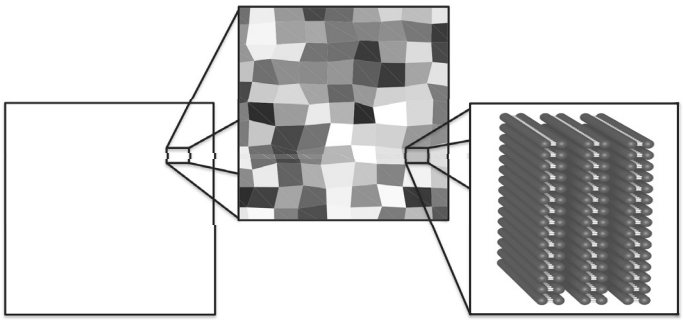

Figure 2.2: Illustrations of different length scales for a lamellar phase. On the left-hand side the resolution is in the mm-scale and the sample appears homogeneous. In the middle, the resolution is in the μm-regime and powder-like features of the sample are observed, the greyscale indicates domains with different orientations of the lamellaes (in each domain all bilayers are parallel to each other). Finally, on the right-hand side the resolution is on the nm-scale and the individual lamellaes, which are $\approx$10 nm thick, can be observed.

picture becomes uniform is λ_{hom}.[8] A further discussion of λ_{hom} using diffusion NMR will take place in section 4.2.1.

Different examples of structures that can be formed are micelles (small spheres where the hydrophobic parts of the surfactants gather in the core and the hydrophilic parts make up a surrounding shell), bilayers (two sheets of surfactants where the tails are oriented towards each other) or bicontinous structures (where both the hydrophilic and hydrophobic parts make networks spanning throughout the sample. Illustrations of the different examples can be found in Figure 2.4

These kinds of structures can be made up of pure polymeric nonionic surfactants (block co-polymers), binary mixtures of surfactants with oil or water and ternary mixtures of surfactant with oil and water. Sometimes co-surfactants or salts are also added.

2.2 Biological Cells

A stack of bilayers is generally referred to as a lamellar phase. Each individual bilayer or membrane acts as a wall or hinderance for the molecules to exchange between the two compartments seperated by the membrane. The most common examples of such a systems are the different types of biological cells that makes up all living things.[9]

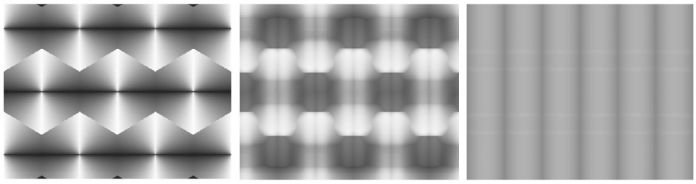

Figure 2.3: An illustration of how details in a picture or structure can be lost as the pixel size or representative length increases. On the one hand one can experience it as how a picture looses its details as the pixel size increases from left to right. On the other hand it could also be seen as the greyscale representing the diffusion direction and how the spins lose track of their direction as they pass through enough parts of the sample, as one goes from left to right. The pixel size for when the details in the picture is lost and the length needed for the spin to diffuse to average over all possible diffusion directions is λ_{hom}.

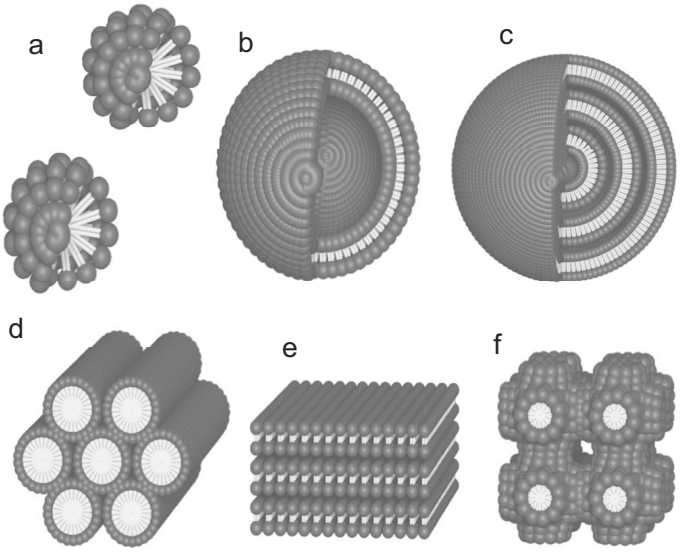

Figure 2.4: Schematic examples of different self-assembly structures, micelles (a), uni-lamellar vesicles (b), multilamellar vesicles (c), hexagonal (d), lamellar (e) and bicontinous structures (f). The dark grey sphere symbolizes the surfactant headgroup while the light grey is the tail of the surfactant. Uni-lamellar vesicles are discussed in paper IV, while multilamellar vesicles (also known as onions) is the topic of paper II. Lamellar phases is the material used in papers I and VII.

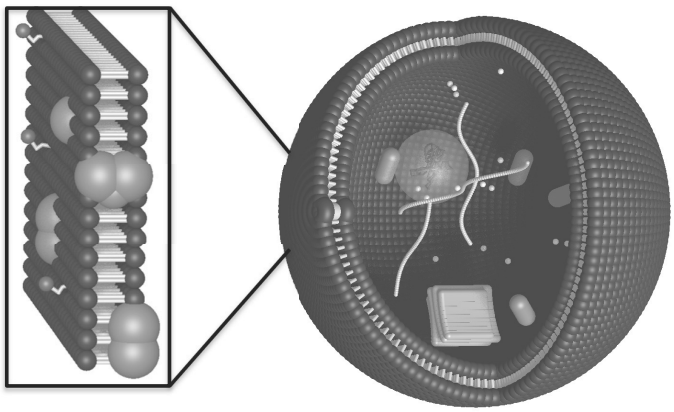

Figure 2.5: Schematic illustrations of the cell membrane (left) and the cell interior (right). In addition to the lipid bilayer the cell membrane includes proteins passing through the membrane (such as aquaporins[1]) and attached to the interface. The interior of a cell includes the nucleus with the DNA bundle, the layered Golgi- apparatus, the cylindrical mitochondria, spherical ribosomes and long microtubules. Note that for clarity a limited amount of the different components present in the membrane and inside the cytoplasm (the interior of the cell excluding the nucleus) are shown. The cell membrane permeability is discussed in paper VI while paper V treats the water diffusion in the intracellular space.

One important thing regarding the cell membrane is that it is comprised of several of different types of polar lipids.[3,9] It also has a lot of proteins stuck to the surfaces and spanning through the bilayer (see left-hand side of Figure 2.5). The inside of a cell is not simple either. Here one finds, amongst other things, the nucleus with the DNA, the ATP-producing mitochondria and the Golgi-apparatus taking care of general production in the cell (see right-hand side of Figure 2.5).

Chapter 3

Diffusion

The spreading out of molecules from their original positions caused by thermal motion is generally referred to as diffusion. This motion exists in all materials with a temperature above absolute zero, but for solids the resulting translational displacements are very small because the energy of interaction is much greater than the kinetic energy and thus the molecules are kept in their lattice places. For liquids and gases, on the other hand, the kinetic energy of the molecules is so much higher than the energy of interaction that it is generally no problem for a molecule to move from its original position.

The translational motion is a random walk. The change in direction is caused by intermolecular collisions and interactions. In many systems a molecule can experience diffusion through three-dimensional space. However, in the NMR methods used in this context one commonly measures diffusion in one specific direction at a time, so in the text that follows the discussion will concentrate on diffusion along one dimension.

Broadly speaking one can identify three types of different diffusion behaviour: free, obstructed and restricted diffusion. The diffusion through a homogeneous medium, passing no boundaries or hindrances, is called free diffusion. If there are obstacles which the molecules can not pass through but have to go around, the molecules are experiencing obstructed diffusion. Restricted diffusion is when the molecules are trapped and have a limited space in which they can move. If the restricting walls are permeable, implying that the molecules can pass the boundaries with a certain probability, it is still generally referred to as restricted diffusion. A schematic picture of these situations is given in Figure 3.1

One thing to notice from Figure 3.1 is that what is characterized as restricted or obstructed diffusion on a certain time-scale could appear as free diffusion on another time-scale. If the diffusion appears to be free it

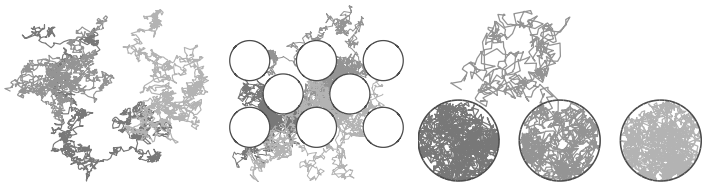

Figure 3.1: Illustrations of trajectories (in 2D) for diffusion under free (left), obstructed (middle) and restricted (right) conditions. Three different trajectories, indicated by different greyscale, are given for each case. For free diffusion the molecules can go anywhere and their paths overlap a lot. The case of obstructed diffusion is here illustrated by white circles into which the molecules cannot enter and have to pass around. The restricted diffusion is illustrated through two cases; in the middle the molecules experience certain permeability and gets the opportunity to penetrate the restriction walls while beside the molecules are trapped within the circles and can not penetrate out at all.

is often referred to as Gaussian diffusion to indicate that it appears to be free but it is not certain that it is. A further discussion on the time dependence of the diffusion takes place in section 3.2 and 3.3.

3.1 Free Diffusion

Free diffusion is characterized by a pure random walk trajectory, see Figure 3.1. During a time step τ, the molecule has moved a characteristic length λ in any direction. The trajectory is characterized by a total time t and a travelled distance $Z = z_t - z_0$, where z_0 is the position at time 0 (the start of the trajectory) and z_t is the position at time t.

The probability density for a molecule to move a distance Z during time t is given by the propagator:

$$P(Z,t) = (\frac{2\tau}{\pi t\lambda^2})^{\frac{1}{2}} e^{-\frac{Z^2\tau}{2t\lambda^2}} \tag{3.1}$$

Examples of $P(Z,t)$ can be seen in Figure 3.2. Embedded in equation 3.1 is the fact that the propagator depends on the time step τ and the characteristic length λ needed to describe the random walk, or rather the ratio $\frac{\tau}{\lambda^2}$. The inverse of this ratio defines the diffusion coefficient for the individual molecule:

$$D_t = \frac{\lambda^2}{2\tau} \tag{3.2}$$

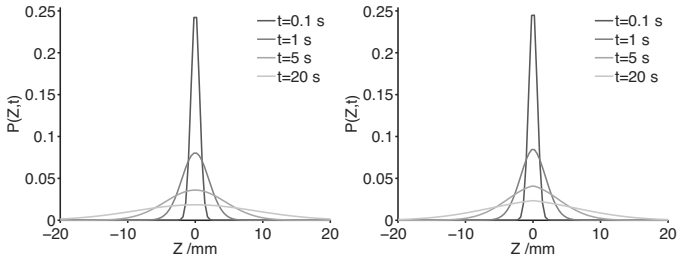

Figure 3.2: Illustrations of propagators for free diffusion on the left-hand side and restricted diffusion on the right-hand side. To calculate these propagators $\tau = 1$ ms and λ was adjusted so that $D_t = 2 \cdot 10^{-9}$ m^{2}s^{-1}. The restricted diffusion is confined to a space of 40 mm in the z-direction. As can be noticed the propagator for the restricted diffusion obtains a triangular shape for the longer times.

Here the subscript t has been used to emphasis that the displacement is monitored through time.

When investigating a macroscopic system, it is in general not possible to measure each trajectory individually but the square root of the mean squared displacement (MSD,$\langle Z^2 \rangle$) during a time t is easier to measure. This quantity is related to the diffusion coefficient for the system through:

$$\langle Z^2 \rangle = 2D_t t \tag{3.3}$$

3.2 Obstructed Diffusion

A molecule diffusing in a volume filled with obstructing objects can generally diffuse quite large distances. However, the observed mean square displacement for a given t will be smaller than that for the case of free diffusion. To clarify that the observed diffusion coefficient is not the same as the diffusion experienced in the bulk of the medium one generally uses the term apparent diffusion coefficient (ADC).[10] The obtained value of the ADC could for small time be slightly time dependent (if the molecule gets trapped between the obstructing objects for a short time, an example is the darkest trajectory in the middle of Figure 3.1) but will for long enough times be independent of time (when the times being trapped are small compared to the whole time of diffusion, as for example the least dark trajectory in Figure 3.1).

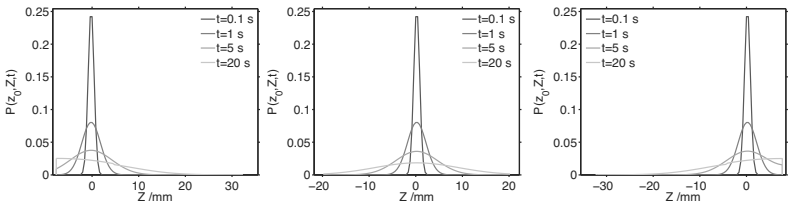

Figure 3.3: Illustrations of boundary effects in the shape of the propagator. On the left-hand side there is a boundary close by as z decreases ($z_0 \approx -12$mm) while on the right-hand side is a boundary in the direction of increasing z ($z_0 \approx 12$mm). In the middle the diffusing molecule is well away from the boundaries and they are not affected by the boundary ($z_0 \approx 0$ mm).

For obstructed diffusion the shape of the propagator changes and becomes more dependent on time t and starting position z_0. Being close to an obstructing object influences the possible paths for the molecule, especially for short times (compare Figure 3.3). For long enough times the obstructing walls will have averaged out and the propagator will have a similar shape as that for free diffusion but being narrower for otherwise identical conditions.

As mentioned above, the propagator for an individual molecule will depend on the starting position of the molecule in question. This is addressed in Figure 3.3. Thus one defines an average propagator for the whole system:[11]

$$\bar{P}(Z,t) = \int \rho(z_0) P(z_0, z_0 + Z, t) dz_0 \tag{3.4}$$

where $\rho(z_0)$ is the spin density at z_0.

3.3 Restricted Diffusion

When measuring the diffusion coefficient one often measures the displacement of molecules with time and by using equation 3.3 one then obtains D_t. Determining the diffusion coefficient in a system with restriction is not a trivial task and will depend on the time t used for the molecules to move, compare Figur 3.4. If t is short the molecules will not have time to experience the confinement and the diffusion will appear as free diffusion and D_t in equation 3.3 will be independent of time. This diffusion coefficient is often denoted D_0. For intermediate times the distance travelled by the molecule will not change much even if the time is increased. The

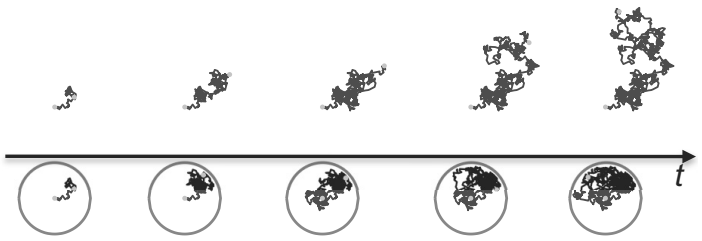

Figure 3.4: A 2D illustration to show the effects of restrictions on displacement. Above the timeline the diffusion is free while underneath it is confined to a circle. The measured displacement is the distance between the starting and ending positions, marked by grey points. For short times the displacement is basically the same for both cases, but as time increases the displacement becomes independent of time in the confined case while it will increase with time for the case of free diffusion.

calculated diffusion coefficient using equation 3.3 will in this case depend on time. When going to long enough times for permeable systems the calculated D_t from equation 3.3 again becomes independent of time. This long-time and long-range diffusion coefficient is often represented by D_∞.

For restricted diffusion the measured diffusion coefficient will thus have a time dependence from which morphological information can be obtained.[12–17] For idealized geometries we have (see Figure 3.5):

$$D_t(t) = D_0\alpha + \frac{2(1-\alpha)}{t}\sum_{m=1}^{\infty}\frac{1-e^{-\alpha_m^2 D_0 t}}{\alpha_m^2(\alpha_m^2 R^2 + 1 - d)} \tag{3.5}$$

where d indicates the dimensionality of the pore geometry (1 for planar, 2 for cylindrical and 3 for spherical), $2R$ is the diameter or plane distance, $\alpha = \frac{D_\infty}{D_0}$ is the inverse tortuosity which conveys information about the combination of restriction shape and connectivity and α_m is the mth root of:

$$J_{\frac{d}{2}}(\alpha_m R) - \alpha_m R J_{1+\frac{d}{2}}(\alpha_m R) = 0 \tag{3.6}$$

where J_ν is the νth order Bessel function of the first kind.

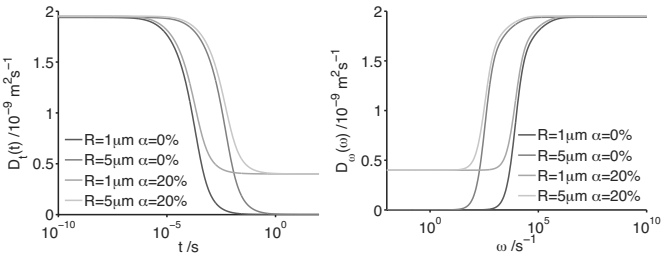

Figure 3.5: Examples of equation 3.5 (left) and 3.9 (right). To generate these graphs D_0 was set to $2 \cdot 10^{-9}\mathrm{m}^2\mathrm{s}^{-1}$ and d to 3.

3.4 Velocity Autocorrelation/Diffusion Spectrum

Instead of monitoring position over time one can monitor velocity over time, or rather the velocity autocorrelation function (VAF , $\langle v(0)v(t)\rangle$).[18,19] This function indicates how the velocity at time t depends on the initial velocity at time 0. The relation between the MSD and the VAF is:[20]

$$\langle Z^2\rangle = 2\int_0^t \int_0^{t'} \langle v(0)v(t'')\rangle dt'' dt' \tag{3.7}$$

The VAF is related to the diffusion phenomenon through the diffusion spectrum:

$$D_\omega(\omega) = \int_0^\infty \langle v(0)v(t)\rangle e^{i\omega t} dt \tag{3.8}$$

Equation 3.8 implies that, the measured diffusion coefficient in general depends on the frequency (ω). This frequency dependence contains information about the sample morphology. For porous media this dependence is, again for some idealized geometries (see Figure 3.5):[20,21]

$$D_\omega(\omega) = \alpha D_0 + (1-\alpha)D_0 \sum_{k=1}^{\infty} \frac{A_k B_k \omega^2}{A_k^2 D_0^2 + \omega^2}. \tag{3.9}$$

The two coefficients A_k and B_k depend on the geometry:

$$A_k = \left(\frac{\alpha_k}{R}\right)^2 \tag{3.10a}$$

$$B_k = \frac{2(R/\alpha_k)^2}{\alpha_k^2 + 1 - d} \tag{3.10b}$$

where d, R and α are the same as for equation 3.5 and α_k is the kth root of:

$$\alpha_k J_{\frac{d}{2}-1}(\alpha_k) - (d-1) J_{\frac{d}{2}}(\alpha_k) = 0 \tag{3.11}$$

where J_ν is the νth order Bessel function of the first kind.

Before moving on to the technicality of measuring the diffusion coefficient, notice the similarities and differences between $D_t(t)$ in equation 3.5 and $D_\omega(\omega)$ in equation 3.9, along with Figure 3.5 . From both these equations and the figure it is clear that the measured diffusion coefficient depends on the used time/frequency and that this dependence can be used to obtain sample structure information. One should note that equation 3.5 and 3.9 are similar from a theoretical point of view. In practice, generally one description is better than the other, depending on system and measurement technique. A further discussion on this will take place in section 4.2.

Chapter 4

Nuclear Magnetic Resonance

Nuclear magnetic resonance (NMR) is a technique with many technical dimensions and levels of complexity.[22,23] It is based on the effects of a magnetic field on the spin angular momentum. This phenomenon is generally treated with the equations of quantum physics. The magnetic field is generated and changed using coils designed by knowledge of electronics. The generated signal can be used to, for example, monitor diffusion behaviour, generally treated within statistical mechanics, or molecular structure, often used in organic chemistry.

Here the focus will be on how to measure diffusion with NMR, both the basics to understand it and some applications. The chapter ends with a short section about spatially resolved NMR, also known as magnetic resonance imaging (MRI).

4.1 Basic NMR

The general description of the NMR phenomena uses tensor analysis. However, by choosing the axes carefully one can (for nuclei with spin $\frac{1}{2}$) use ordinary vector analysis. To avoid complications this kind of simplification has been done throughout this section.

We start with a short introduction to the origin of the NMR signal and radio frequency (RF) pulses, move on to the chemical shift and finish with the relaxation phenomena.

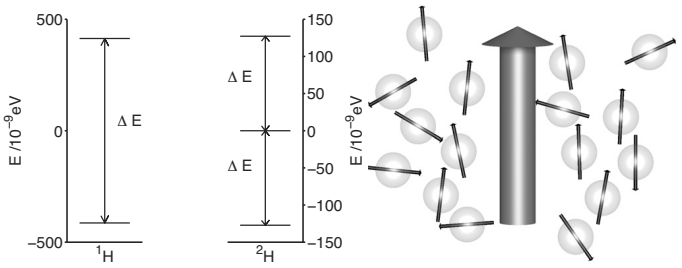

Figure 4.1: On the left-hand side are the energy levels and the allowed transitions for ^{1}H and ^{2}H nuclei in a magnetic field of 4.7 T. On the right-hand side is an illustration of the nuclear magnetic moments and the resulting magnetization vector (large grey arrow) in a magnetic field directed upwards.

4.1.1 Origin of the signal

The projection of the spin angular momentum, **I**, onto the z-axis, I_z, is a quantized property:

$$I_z = m\hbar \tag{4.1}$$

where $\hbar$ is the reduced Planck's constant and m is the magnetic quantum number. m can take $2I+1$ values, where I is the spin quantum number. I is a non-negative multiple of one half, most common are $\frac{1}{2}$, 1 and $\frac{3}{2}$. In this work only proton (^{1}H) and deuterium (^{2}H) are considered. For these two nuclei I is $\frac{1}{2}$ and 1, respectively.

The magnetic momentum, μ, is related to I_z through:

$$\mu = \gamma I_z \tag{4.2}$$

where γ is the gyromagnetic ratio, a property of the nuclei.

When a nucleus with a magnetic moment is affected by a magnetic field, B, it experiences a shift in energy levels:

$$E = -\mu B = -m\hbar\gamma B. \tag{4.3}$$

By convention, the magnetic field is directed along the z-axis.

In NMR the only allowed transitions are $\Delta m = \pm 1$ and the energy of radiation is $\Delta E = h\nu$ (where $\nu = \frac{\omega}{2\pi}$). Thus:

$$\Delta E = \hbar\gamma B = h\nu \Rightarrow \nu = \frac{\gamma B}{2\pi} \tag{4.4}$$

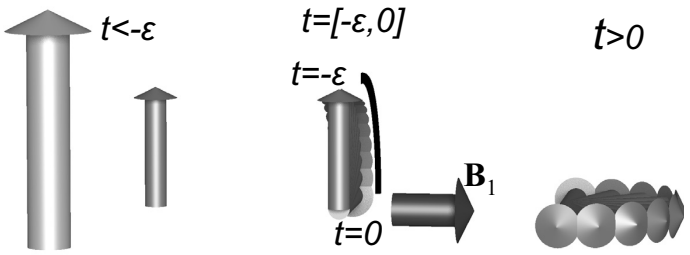

Figure 4.2: An illustration of the effect of a 90°-RF-pulse applied at $t = -\varepsilon$ on $\mathbf{M}$. $\mathbf{B}_0$ is indicated through the large arrow to the left. At $t < -\varepsilon$, e.g. at equilibrium before the pulse, $\mathbf{M}$ is directed along $\mathbf{B}_0$. During the pulse, here illustrated with $\mathbf{B}_1$ as a dark arrow, $\mathbf{M}$ flips to the transverse plane. The duration of the pulse ε is generally short, 5-30μs. Traditionally $t = 0$ is used for the time directly after the pulse. After the pulse, $t > 0$, $\mathbf{M}$ precesses around $\mathbf{B}_0$ in the transverse plane.

By sending electromagnetic waves with a specific frequency one excites the nuclei fulfilling the resonance condition in equation 4.4, while the rest are left unchanged.

4.1.2 Radio frequency pulses

At equilibrium the overall magnetization, $\mathbf{M}$, of a sample is pointing along the external magnetic field, $\mathbf{B}_0$, see Figure 4.1. By convention the direction of the magnetic field is denoted z and is called the longitudinal axis. The perpendicular x,y-plane is called the transverse plane.

In the presence of a magnetic field the nuclear angular momentum rotates around the direction of the magnetic field. The frequency for this precession is referred to as the Larmor frequency:

$$\omega_0 = \gamma B_0. \tag{4.5}$$

Through a pulsed electromagnetic wave, also known as a radio frequency or RF-pulse, a temporary magnetic field, $\mathbf{B}_1$, perpendicular to the external field is created and the magnetization of the nuclei with the right resonance frequency is flipped by precessing around $\mathbf{B}_1$. These RF-pulses are characterized by the angle with which they flip the magnetization around $\mathbf{B}_1$. The example given in Figure 4.2 is called a 90°-pulse.

The signal measured is proportional to the magnetization in the transverse plane. Combinations of pulses, with similar or different flip

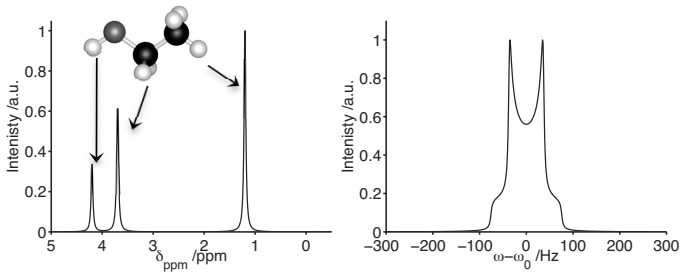

Figure 4.3: Schematic proton spectrum for ethanol (left) and deuterium spectrum for deuterated water in a lamellar phase (right). Both these spectra are calculated, taking only into account effects due to the shielding (for the proton spectrum) and quadrupolar coupling (for the deuterium spectrum). For the proton case an illustration of the ethanol molecule is included and the type of proton generating each peak is indicated.

angles, are called pulse sequences and are often used to compensate for different imperfections in the instrument and/or to extract a certain part of the magnetization.[24]

4.1.3 The spectrum

The measured signal over time is a superposition of the contribution from the different nuclei with resonance frequencies within the frequency range that the spectrometer is set to be detected. By Fourier transorming the measured signal through time a spectrum is obtained. The resonance frequency of each nuclei is indicated by a peak in the spectrum.

As can be deduced form equation 4.4 the resonance (or excitation) frequency of a specific nucleus is dependent on the magnetic field it is experiencing. The magnetic field influencing the nuclei can be divided into two parts, one external field, B_0, which is applied from outside the sample, and one internal part, which is due to the nearby surrounding, such as electron clouds and other nuclei influencing the magnetic field.[23]

The internal part of the magnetic field caused by the electrons is referred as shielding, σ. If σ is positive it decreases the applied magnetic field:

$$\omega = \gamma B_0(1 - \sigma) \tag{4.6}$$

The other contribution to the internal part of the magnetic field comes from the interaction with nearby nuclei, called nuclear spin-spin coupling.

This interaction can either be through space, known as direct dipole-dipole coupling, or through the electron bonds, known as J-coupling or indirect dipole-dipole coupling. Rather then shifting the whole peak through the spectrum a coupling contribution splits the peak keeping the central position constant.

The displacement of resonance frequency through the spectrum is generally called chemical shift. When discussing this phenomena one generally uses a ppm-scale obtained using a reference frequency ω_{ref}:

$$\delta_{ppm} = 10^6 \frac{\omega - \omega_{ref}}{\omega_{ref}} = 10^6 \frac{\sigma_{ref} - \sigma}{1 - \sigma_{ref}} \tag{4.7}$$

A clear advantage to use δ_{ppm} is that it is generally independent of the magnetic field (one exception is the influence of quadrupolar interactions discussed below). So the position of the different peaks in the spectrum for a specific compound will be the same, regardless of which spectrometer was used. The shape of the peaks could, however, be slightly different because of resolution and relaxation differences (amongst other things).

For most common molecules containing hydrogen δ_{ppm} spans between 0 and 10 ppm in a proton spectrum. An example of a proton spectrum is given in Figure 4.3.

It should be noted that the chemical shift depends on the orientation of the molecule in respect to the external magnetic field. In isotropic liquids this is generally not an issue because the molecules tumble around (usually on the ns time-scale) so that all orientations have been sampled during the acquisition of the signal (usually on the ms time-scale) and a narrow peak appears in the spectrum. For anisotropic samples, where there is a directionality in the sample (as for example a lamellar or hexagonal phase, see Figure 2.4) complete averaging does not take place and each orientation of the liquid crystalline microdomains contributes with its own frequency. The shape and width of the resulting spectrum thus depends on the details of molecular reorientation within each microdomain, and the distribution of microdomain orientations.

For nuclei with $I > \frac{1}{2}$ an interaction called quadrupolar coupling is a dominant factor for the appearance of the spectrum. By using deuterated water and quadrupolar couplings information on the phase of the sample can be obtained. If all orientations are present in a lamellar phase made using D_2O the deuterium spectrum will appear similar to the one presented in Figure 4.3 (also known as a Pake-pattern).[25,26] The shift between the two main peaks or "horns" is often referred to as the quadrupolar splitting $\Delta\nu$.

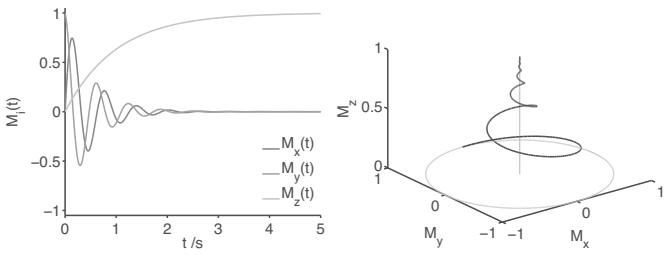

Figure 4.4: An illustration on how the different components of the magnetization vector depends on time after a 90°-pulse (on the left-hand side) and the dependence on time for the actual vector **M** (on the right-hand side). The curves were obtained using equations 4.8 and 4.9 along with the parameter values: $M_{eq} = 1$, $T_1 = 1$s, $T_2 = 0.5$s and $\omega = 10\text{s}^{-1}$. Note that the value for T_1 and T_2 are realistic values for liquid-like samples, while the value for ω is chosen so that the oscillation of M_x and M_y are observed in the illustrations. In the graph of the right-hand side two greyish lines have been added to guide the eye. These are the circle for the plane at $z = 0$ using a radius of M_{eq} and the line in the z-direction originating from the origin of the coordinate system.

4.1.4 Relaxation

A simple way to look at the relaxation phenomena is that the magnetization spreads out in the sample and thus returns to equilibrium. It is the fluctuations in the interactions between the spins and their environment that determine the relaxation. Thus, the spins tumbling and translational motion contributes to the relaxation rates.

The longitudinal relaxation along the z-axis after an excitation is often called T_1-relaxation. T_1 is the constant in the exponential increase for the magnetization in the z-direction, which after a 90°-pulse is:

$$M_z(t) = M_{eq}(1 - e^{-\frac{t}{T_1}}) \tag{4.8}$$

where M_{eq} is the magnitude of the magnetization at equilibrium.

In the transverse plane the magnetization rotates and experience a transverse relaxation, also known as a T_2-relaxation. The magnetization in the x and y-direction changes after a 90°-excitation pulse according to:

$$M_x(t) = M_{eq}\sin(\omega t)e^{-\frac{t}{T_2}} \tag{4.9a}$$

$$M_y(t) = M_{eq}\cos(\omega t)e^{-\frac{t}{T_2}} \tag{4.9b}$$

The effect of relaxation on the magnetization is shown in Figure 4.4.

4.2 Measuring Diffusion

As can be deduced from equation 4.5 the precession frequency of a spin's magnetic momentum depends on the strength of the magnetic field it is experiencing. By making the strength of the magnetic field depend on position one can thus label the spins with respect to position.

In pulsed field gradient (PFG) NMR one applies temporary magnetic field gradients in the, otherwise, homogeneous magnetic field to "mark" the position of the spins. After a pulse the spins will go back to precess with the same frequency as before the gradient pulse but because of the gradient pulse the spins have aquired a phase being linearly dependent on their position, see Figure 4.5. After a certain time, called the diffusion time, a second gradient is applied with the same strength and duration, but with opposite direction. The purpose of this second pulse is to oppose the phase difference caused by the first pulse, thus trying to "de-mark" the spins. If they are in the same position during both pulses, the magnetization phase once again becomes equal throughout the sample and the signal intensity is fully restored. On the other hand, if diffusion, or any other translational motion, has taken place the effects of the first and second gradient pulses do not cancel each other. This leads to all spins not having the same phase and the signal intensity decreases. The parameter being observed with NMR is actually $\langle Z^2 \rangle$.[27,28]

For a sample experiencing no other translational motion than gaussian diffusion, the measured intensity is given by:

$$S(b) = S_0 e^{-bD} \tag{4.10}$$

where D is the measured diffusion coefficient, b is a parameter depending on the time evolution of the magnetic field gradient (a more detailed discussion of b follows in section 4.2.1 and 4.2.2) and S_0 is the signal intensity for $b = 0$. S_0 depends mainly on relaxation so by keeping the echo time (the time between the excitation pulse and the acquisition of the signal) constant one often uses a normalized intensity $E(b) = \frac{S(b)}{S_0}$.

If the diffusion contains more than one contribution the intensity will be a superposition of the different components present in the system:

$$E(b) = \sum_j f_j e^{bD_j} \tag{4.11}$$

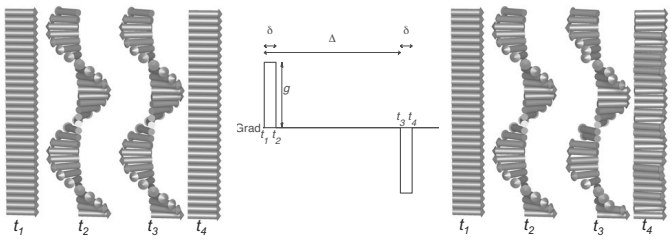

Figure 4.5: The effect of the gradient pulses (an example of a basic gradient sequence is shown in the middle) on the magnetization without diffusion (left) and with diffusion (right). No excitation pulse is included but it is presumed that the magnetization is already in the transverse plane. Before the first gradient pulse, t_1, the phase of the magnetization is the same throughout the sample. After the second pulse, t_2, the gradient has made the phase of the magnetization spatially dependent. Between the two gradient pulses, nothing happens if there is no diffusion while if diffusion is taking place the helix of the magnetization created by the first pulse gets distorted. The second pulse is identical to the first except having an opposite sign, so if no diffusion has taken place it totally compensates the first pulse and unwinds the magnetization helix at t_4. If, on the other hand, diffusion has taken place the compensation is not complete and the magnetization phase is not uniform, causing a decrease in the measured signal.

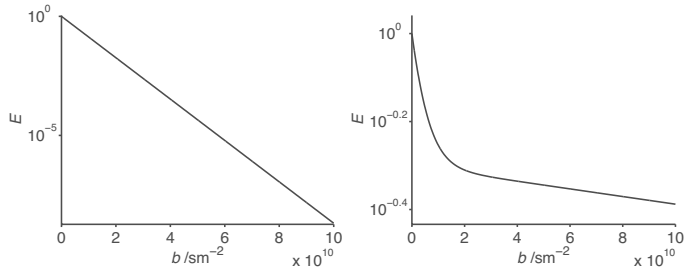

Figure 4.6: An example of a single exponential decay (left) and a bi-exponential decay (right). Examples for when single exponential decay is observed are free diffusion and obstructed diffusion if long enough Δ are used. Bi-exponential decays are, for example, observed for molecules which can be both "fast" and "slow" in the same sample (as in the case for a cell suspension, see paper V and VI or slow exchange for ligand binding) and when two molecules with large size difference is observed in the same decay. The single exponential decay was produced using $D = 2 \cdot 10^{-10}$ m^{2}s^{-1} while for the bi-exponential decay $D_1 = 2 \cdot 10^{-10}$ m^{2}s^{-1}. $D_2 = 2 \cdot 10^{-12}$ m^{2}s^{-1} and $f_1 = 0.5$ (see equation 4.11).

where f_j is the fraction of component j and D_j is the measured diffusion coefficient for component j. Examples of what could be different components are given in the caption of Figure 4.6.

For the sequence shown in the middle of Figure 4.5:

$$b = (\gamma g \delta)^2 (\Delta - \frac{\delta}{3}) \tag{4.12}$$

where γ is the gyromagnetic ratio, g is the strength of the magnetic field gradient, δ is the duration of the gradient pulse and Δ is the time between the start of the two gradient pulses. The second parenthesis on the right-hand side is generally known as the effective diffusion time, t_d, where $\frac{\delta}{3}$ compensates for the finite duration of the gradient pulse.

The way to measure the diffusion coefficient or displacement is thus to change the strength or duration of the applied gradient pulse or the effective diffusion time in a systematic way, see Figure 4.6. The most common is to change the gradient strength. There are two main reasons for this: the choice of varying the times δ or t_d can influence the results if any obstruction or restriction in the diffusion is present[29] and it is complicated to deal with relaxation effects. The duration of the gradient pulse influences the results because the position marked is the time

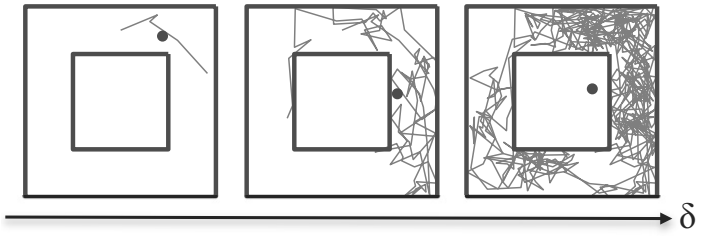

Figure 4.7: An illustration on how the length of δ can influence the position marked by the gradient pulses. The spin trajectories are confined to a square shell (marked with thick black lines). The black circles indicate the averaged position during the gradient pulse. From left to right the duration of the pulse increases and one can see that the as the length of the pulse increases the marked position becomes less representative of where the spin has actually been.

average position of where the spin has been during the gradient pulse, see Figure 4.7.[30–36] The time between the pulses sets the diffusion time and thus influences according to equations 3.5 and 3.9, where t is the diffusion time. Note that equation 3.5 is only valid for extremely short pulse durations, short enough for restrictions not to influence the measured diffusion. The equation for the dependence of $\langle Z^2 \rangle$ on δ and t_d for ideal non-permeable geometries is (see also paper V):

$$\begin{aligned} \langle Z(\delta, t_d)^2 \rangle &= 4 \sum_m^\infty \frac{1}{\alpha_m^2 (\alpha_m^2 R^2 + 1 - d)} \\ &\times \frac{2\alpha_m^2 D_0 \delta - 2 - 2L(\delta) + 2L(t_d + \frac{\delta}{3}) - L(t_d - \frac{2\delta}{3}) - L(t_d + \frac{4\delta}{3})}{\alpha_m^2 D_0 \delta^2} \end{aligned} \tag{4.13}$$

where α_m, R, d and D_0 are the same as for equation 3.5 and $L(t) = e^{-\alpha_m^2 D_0 t}$.

In this introduction the text has concerned PFG. Of course, one could just as well use steady gradients and flip the magnetization vector of the spins through a 180°-RF-pulse (making $\Delta = \delta = \tau$, where τ is the time between the excitation pulse and the 180°-pulse). A common way of doing diffusion NMR is to combine PFG with different sequences of RF-pulses.[37–39] In this way one can avoid and compensate for imperfections in the instrument, such as inhomogenieties in B_0 and B_1 along with unequal gradient pulses in opposite directions. These methods can also make it easier to control and/or use relaxation effects or signal from

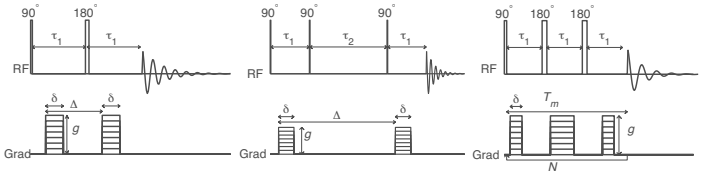

Figure 4.8: Three sequences for measuring diffusion; PGSE (left), PGSTE (middle) and MGSE (right). The upper panel shows the RF-pulses used while the lower illustrates the gradient pulses with varying amplitudes. During the times indicated with τ_1 transverse relaxation takes place while during the times indicated with τ_2 longitudinal relaxation occurs. The loop in the MGSE is included to show that the same sequence is carried out N times.

specific spins. Below follows the discussion of two major types of these combined pulse sequences followed by a section on filter exchange spectroscopy.

4.2.1 Pulsed Gradient Spin Echo

The two most commonly used experiments for determining molecular displacements are the pulsed gradient spin echo (PGSE)[37] and the pulsed gradient stimulated echo (PGSTE).[38]

As can be seen in Figure 4.8 they are quite similar, the only difference is that the 180°-pulse in the PGSE-experiment corresponds to two 90°-pulses separated by a time τ_2 in the PGSTE-experiment. This difference makes the PGSE-sequence more sensitive to T_2-relaxation and the the PGSTE-sequence more sensitive to T_1-relaxation. Since the relaxation parameters depend on the surrounding of the nuclei it is the nature of the sample that determines which sequence is preferred.

For this family of PFG-experiments:

$$b = \gamma^2 \int_0^t \left(\int_0^{t'} G(t'')dt'' \right)^2 dt' \tag{4.14}$$

Note that $G(t)$ is the time function for the gradient experienced by the spins which is not always the same as the applied gradient, compare Figures 4.5 and 4.8. For the PGSE- and PGSTE-sequences shown in Figure 4.8 equation 4.12 can be used. It should be mentioned that different shapes of the gradient pulses (not just rectangular as shown in the Figures 4.5 and 4.8) can be used, which influences the calculation of b.

With the PGSE- and PGSTE-experiment one monitors the time dependent diffusion coefficient D_t. Thus, equation 3.5 and the other equations presented in paper V can be used.

It is customary to use an experimental parameter q, instead of b, which is defined as:[40]

$$q = \frac{\gamma g \delta}{2\pi} \tag{4.15}$$

The parameter q is an inverse length and is thus a wave vector. By plotting E against q structural information can be obtained, in different ways.In one of the techniques short gradient pulses are used. Then the normalized intensity dependence on q is:[41–47]

$$E(q, t_d) = \int P(Z, t_d) e^{i2\pi q Z} dZ \tag{4.16}$$

and in the limit $t_d \to \infty$, that is to say when the molecules have time to migrate throughout the sample:

$$E(q, \infty) = \mathsf{FT}\{P(Z, \infty)\} = |\mathsf{FT}\{\rho(z)\}|^2 \tag{4.17}$$

where $\rho(z)$ is the spatially dependent density and FT indicates a Fourier transform.[48–51]

In principle, by doing an inverse Fourier transform of the echo decays one can obtain structural information. However, it should be noted that a short δ is generally needed and unless very ideal, characteristic distances are present, interpreting the result is not trivial. In ideal structures the sample gives rise to diffraction effects from which structural information can be obtained directly, see left-hand side of Figure 4.9.[52,53]

Another technique is the one presented in papers I, II and IV. In this method one compares the echo decys for different values of δ but keeping the used t_d and q values the same. In this way one can compare two regions of q (two different length-scales); for small q (equivalent to large length-scales) the decays are independent of δ and fall together while for large q (equivalent to short length-scales) the decays depend on δ, see right-hand side of Figure 4.9. For long distance, or low resolution, any structural information is lost while for short distances, or high resolution, the structure effects the signal. This could be compared to the length-scale influences shown in Figure 2.2 or resolution details lost in Figure 2.3. The inverse of the q value for which the decays go from being independent to dependent of δ is defined as λ_{hom}, see also section 2.1. However, for λ_{hom} to be well defined the spins need to be able to monitor

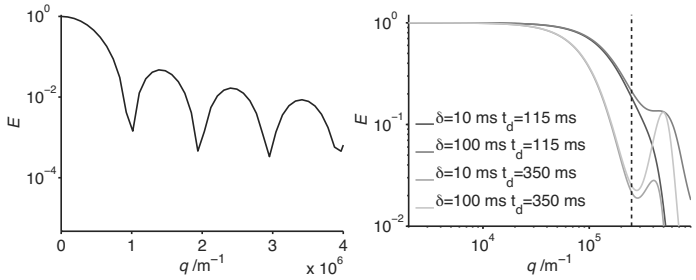

Figure 4.9: An example of the diffraction pattern for an echo decay (left) and an example of the influence of changing δ (right). For the diffraction pattern a single slit with a wall distance of 1 μm was used. For the dependence of δ the data has been taken from the simulations of diffusion in permeable shells done in paper II. The dashed line indicate the q-value for which λ_{hom} is obtained.

a representative volume of the sample, so t_d has to be long enough for this to be achieved.

4.2.2 Modulated Gradient Spin Echo

During a modulated gradient spin echo (MGSE) experiment the frequency of the applied gradient is used:[18,19,54]

$$b = |\gamma \int_0^t \int_0^{t'} G(t'')dt''e^{i\omega t'}dt'|^2 \tag{4.18}$$

Just as in equation 4.14 $G(t)$ is the time function for the gradient experienced by the spins.

An example of a MGSE-sequence is shown on the right-hand side of Figure 4.8. For this sequence:

$$b = (\gamma g \delta)^2 \frac{t_e}{2} \tag{4.19}$$

where t_e is the echo time and thus the product of N, the number of periods, and T_m, the time needed for one period. By using different T_m (keeping t_e constant to avoid relaxation effects) one obtains the frequency dependence of the diffusion coefficient. Using equation 3.9 one can thus obtain structural information. Note that, just as in the case of time dependent diffusion (see discussion of equation 4.14), more complicated gradient pulse shapes and sequences can be used, which effects the calculation of b.

As can be seen from Figure 4.8 and the discussion at the end of section 3.4 regarding equation 3.5 and 3.9, there are similarities and differences between the PGSE- and MGSE-experiments and analysis. For technical reasons there are lower limits for τ_1, τ_2 and δ and thus for Δ and T_m. As a consequence, the PGSE-experiment is generally better for long times and long-range diffusion while the MGSE-experiment is often preferred for short times and short-range diffusion. This makes the two techniques ideal to combine so that they complement each other, as was done in paper IV.

To obtain structural information for a sample some prior knowledge is needed for both techniques, for example which d to use in equation 3.5 and 3.9. Combining the two techniques can also help making appropriate choices for which model to use when fitting the data to obtain reasonable values for model parameters, even if no prior knowledge exists.

4.2.3 Filter Exchange Spectroscopy

To measure exchange or permeability two things are crucial, one has to be able to identify and seperate the species from the two compartments and in some way be able to follow the evolution of one, or both, through time. For permeable restrictions these species can be identified as "fast" and "slow" diffusing species in a PGSE-experiment. The "fast" diffusion originate from the medium surrounding the confinements, here the diffusion could be obstructed but should be quite similar to bulk. The "slow" diffusion originates from the medium inside the restrictions, which because of the confining walls will have a low ADC.

Remembering that the echo decay is a superposition of the contributing components, see equation 4.11, the time dependence for E_i in a two component system including exchange can be written as:[55]

$$\frac{dE_f}{dt} = -\gamma^2 g^2 \delta^2 D_f E_f - \frac{E_f}{\tau_f} + \frac{E_s}{\tau_s} \tag{4.20a}$$

$$\frac{dE_s}{dt} = -\gamma^2 g^2 \delta^2 D_s E_s - \frac{E_s}{\tau_s} + \frac{E_f}{\tau_f} \tag{4.20b}$$

where the subscript f and s stand for the component experiencing "fast" or "slow" diffusion, respectively. E_i is the normalized echo decay for component i, D_i is the diffusion coefficient for component i and τ_i is the exchange time for component i, i.e. the mean residental time for a spin to be in the compartment containing component i. This coupled differential equation has a solution:

$$E(t_d) = E_f(t_d) + E_s(t_d) = f'_f e^{-\gamma^2 g^2 \delta^2 D'_f t_d} + f'_s e^{-\gamma^2 g^2 \delta^2 D'_s t_d} \tag{4.21}$$

where

$$D'_{\substack{f\\s}} = \frac{1}{2}\left\{ D_f + D_s + \frac{1}{\gamma^2 g^2 \delta^2}\left(\frac{1}{\tau_f} + \frac{1}{\tau_s}\right) \pm \left[\left\{ D_s - D_f + \frac{1}{\gamma^2 g^2 \delta^2}\left(\frac{1}{\tau_s} - \frac{1}{\tau_f}\right)\right\}^2 + \frac{4}{\gamma^4 g^4 \delta^4 \tau_f \tau_s}\right]^{\frac{1}{2}}\right\} \tag{4.22}$$

and

$$f'_s = \frac{1}{D'_s - D'_f}(f_f D_f + f_s D_s - D'_f) \tag{4.23a}$$

$$f'_f = 1 - f'_s \tag{4.23b}$$

Equation 4.21, known as the Kärger model, includes a lot of parameters that need to be known in advance to do a proper fitting to obtain τ_f and τ_s. The choice of t_d is also important for two main reasons: 1) if t_d is short compared to the τ_f and τ_s no exchange will take place during the experiment and determining the exchange times properly will basically be impossible 2) if, on the other hand, t_d is long compared to τ_f and τ_s the exchange could have gone both back and forth thus indicating incorrect exchange times. It should be noted that it is presumed that the exchange is not limited by diffusion, i.e. it is more probable that a molecule reaches the restricting wall than that it passes through it. The advantage of this technique to measure exchange is thus that it is fast, obtaining an echo decay takes just minutes, and an exact number can be estimated through fitting equation 4.21, but it has its limits in the choice of t_d and the knowledge needed to minimize the number of fitting parameters.

Diffusion exchange spectroscopy (DEXSY) is another technique to measure exchange.[56] It combines two PGSE-experiments, for which g is varied independently, with a t_m inbetween, see left of Figure 4.10. By doing a 2D inverse Laplace transformation, where each individual PGSE contributes to one dimension, one can correlate the two diffusion experiments. If cross-peaks show up in between the two components in the 2D-spectrum exchange has taken place during t_m, otherwise no exchange has taken place. This indicates that is is a quite direct technique, either

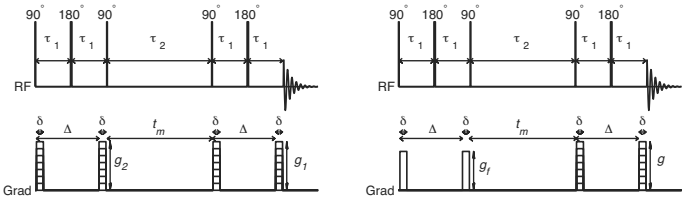

Figure 4.10: The pulse sequence for DEXSY (left) and FEXSY (right). Just as in Figure 4.8 τ_1 indicates time during which transverse relaxation takes place while τ_2 indicates time for which longitudinal relaxation occurs. t_m is the time during which exchange take place. For the DEXSY experiment g_1 and g_2 are changed independently while for the FEXSY g_f is set to an appropriate value to achieve a filter value b_f so that only signal from the "slow" diffusing component remains and g is change as in an ordinary PGSE.

there is exchange during t_m or there is not. Determining the actural exchange time is however not as easy and that is a disadvantage. Another drawback is that a large dataset is needed to make an appropriate 2D inverse Laplace transformation[57] and thus experimental times are long.

A third alternative is the filter exchange spectroscopy (FEXSY) which combines the short experimental time and equations similar to the Kärger model but has the advantage that exchange can be identified as easy as in the DEXSY-experiment. The trick is to reduce the number of diffusion in the DEXSY-sequence and instead include a variation in t_m, see right of Figure 4.10. In this case the first PGSE works as a filter while the second detects the amount of "fast" and "slow" diffusiong component. The change of the fraction of "fast" diffusion component for different t_m is then used to calculate an exchange time.

$$E(b, t_m) = f_f(t_m)e^{-bD_f} + (1 - f_f(t_m))e^{-bD_s} \tag{4.24}$$

where

$$f_f(t_m) = f_f^{eq} - (f_f^{eq} - f_f(0))e^{-kt_m} \tag{4.25}$$

for which $k = k_f + k_s$ is the global exchange rate ($k = \frac{1}{\tau}$) and f_f^{eq} is the fraction of "fast" diffusing component at equilibrium. Practically it is appropriate to include one decay with low b_f and short t_m to get a more accurate value for f_f^{eq}. A theoretical example of how $E(b, t_m)$ and $f_f(t_m)$ could appear experimentallt is shown in Figure 4.11.

It should be noted equation 4.25 and Figure 4.11 this method has the same limits as the Kärger model regarding exchange time and exper-

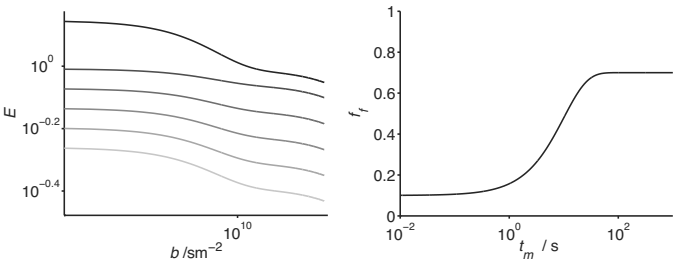

Figure 4.11: An example of how the echo decays and the fraction of "fast" diffusion component can appear for a FEXSY experiment. The different echo decays are shifted using a T_1-relaxation of 5s and is introduced to separate the different decays. The black top decay is the decay for the equilibrium, i.e. using low value of b_f or for $t_m = \infty$, while the rest are for different t_m ranging from 0.1 to 3 s and where $_m$ increases as the decay color becomes lighter. For this example D_f was set to $2 \cdot 10^{-10}$ $\mathrm{m^2 s^{-1}}$, D_s equalled $1 \cdot 10^{-12}$ $\mathrm{m^2 s^{-1}}$. f_f^{eq} was 0.7, $f_f(0)$ indicated a not perfect filter having a value of 0.1 and k had a value of 0.1 s.

imental time, i.e the optimal is to have a range of t_m close to the value of τ which makes sure that the change from low to high f_f can be observed.

4.3 Imaging

The magnetic field gradients can be used to obtain spatially resolved signals.[58,59] These signals can contain any kind of NMR information that will thus be spatially resolved.

Two basic imaging sequences are seen in Figure 4.12. One is called chemical shift imaging (CSI) which maintains the information about the chemical shift by acquiring the signal with the magnetization helix present.[60] The other is called gradient echo (GE) which loses any chemical shift resolution because of the unwinding of the magnetization which is done during acquisition.

By comparing Figure 4.8 and 4.12 one can see a lot of similarities between the diffusion and the imaging sequences. The main difference is that in an imaging experiment the signal is monitored as the winding of the magnetization helix changes while in a diffusion experiment the winding is compensated with the aim to have no spatial dependence when acquiring the signal.

The signal acquired in an imaging experiment is related to real space through a Fourier transform using the wave vector $\mathbf{k}$:

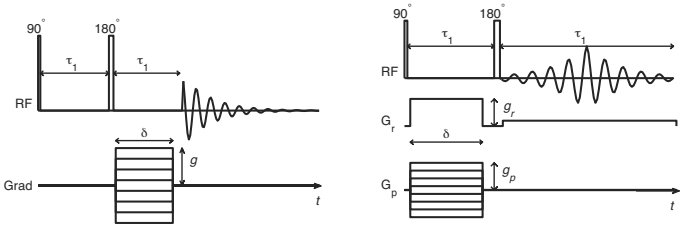

Figure 4.12: An illustration of the pulse sequence for CSI (left) and GE (right). Both sequences are based on the spin echo RF-sequence (90°-τ_1-180°) but it is the gradients that is important for making MR-images. To make a 2D GE-image gardients in two directions are needed. The read direction or dimension is spanned through the second low and long pulse in G_r during which acquisition is also taking place. The other gradient direction G_p is stepped through one position at a time is shown as the phase direction. For a CSI-sequence time during the acquasition is one dimension and the stepping of the gradient is the other.

$$I(\mathbf{r}) = \int S(\mathbf{r}) e^{-i2\pi \mathbf{k}\cdot\mathbf{r}} d\mathbf{r} \tag{4.26}$$

where

$$\mathbf{k} = \gamma \int \mathbf{G}(t) dt \tag{4.27}$$

Note that $\mathbf{G}(t)$ is the gradient felt by the magnetization and is not always oriented the same as the applied gradient shown in the timelines Grad, G_r and G_p in the figures of the pulse sequences, compare Figures 4.5, 4.8 and 4.12. In the case of a 2D GE-sequence this means that equation 4.26 is a 2D Fourier transform with the read and the phase directection as the two dimensions. For the CSI-sequence a 2D Fourier transform is aslo needed but here the dimensions are the direction of the gradient pulse and time.

In Figure 4.13 examples of a CSI-image and a GE-image are shown. The shown images are relatively simple but more complex systems[61] and different contrasts can be used. Applications include measuring changes over time, e.g. in the measuring of the interbilayer forces (as in paper VII) or the slow diffusion of specific species.[62–64] Imaging sequence can also be combined with other NMR-sequences, for example measuring T_1,[65] D[66–68] or λ_{hom} (see section 5.1).

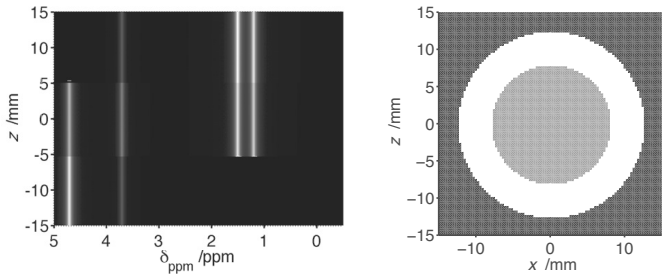

Figure 4.13: Schematic chemical shift image (left) and density image (right). The CSI is illustrating a three phase sample where there is a water-rich phase (with small amounts of surfactant) in the bottom, an emulsion phase (containing water, oil and surfactant) in the middle and an oil-rich phase (with small amounts of surfactant) on top. The density image illustrates the cross-section of an outer-tube filled with pure water with an inner-tube containing 50% water (for example a mixture of water and heavy water in equal amounts).

Chapter 5

Summary of Results

Below follows a short summary of the different projects which make up the main work of this thesis. To avoid repetition and in an attempt to be brief the included articles are categorized into different groups. For obvious reasons, it is not always easy to place an article under one specific label and thus an article can appear in more than one category.

5.1 The homogeneous length scale

Different parts of this project can be found in papers I, II and IV.

As introduced in section 4.2.1 the original way to use q-space, i.e. equations 4.16 and 4.17, presumes very strict conditions to be easily interpreted. The two main conditions are; a well defined distance within the sample and short gradient pulse durations. These conditions could be hard to meet and coherence effects have only been observed for a limited amount of systems.[48,52,69,70] By instead focusing on the dependence of the δ on the echo decays we developed the technique to measure the homogeneous length-scale λ_{hom} using diffusion NMR. This method identifies a transition between the length scale for which the sample appears homogeneous and the length scale for which the sample appears inhomogeneous with regard to the diffusing molecules. It uses the parameter q, which is a wave vector, and the dependence of the echo decay on the used δ. At low q-values the decays are independent of δ. The spins thus monitor a too large distance to experience the details, the sample appears homogeneous. For high q-values the decays are different for different δ. The spins monitors small enough distances to observe the details, the details in the microheterogeneities is detected.

In paper I it is shown that the method can identify lamellar phases

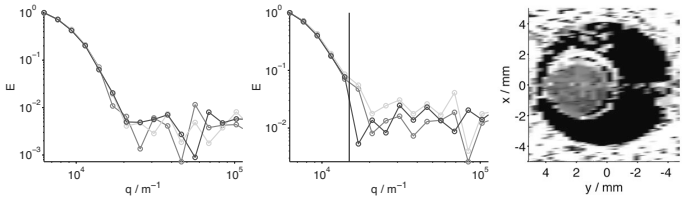

Figure 5.1: The echo decays for a pixel of water (left) and for a lamellar phase (middle) and the resulting GE-image with λ_{hom} as the color-scale (right). For the echo decays the colors indicate different length of δ: 1 (red), 4.5 (green) and 20 (blue) ms. The t_d used for all experiments was 207 ms. For the 2D image the white areas symbolized areas with only noise, while the black areas are the parts containing water and thus has a λ_{hom}=0. The reddish area is the lamellar phase which has a λ_{hom} of $\approx$10 μm.

with different domain sizes. The method was then used for a sheared lamellar phase, paper II, from which an approximate relation between λ_{hom} and the radius of well packed multilamellar vesicles was found. The method was combined with the MGSE to obtain structural information for a vesicle gel. A further discussion on this takes place in section 5.2.

To conclude the project a 2D-image of a tube of a lamellar phase inside a tube of water using λ_{hom} as a contrast was done. The result can be seen in Figure 5.1. It include echo decays for a pixel containing water, a pixel containing lamellar phase and a 2D-image having λ_{hom} as contrast. This shows that it is possible to obtain such an image.

5.2 Chemical Shift Resolution for MGSE

Papers III and IV fall under this category.

Existing literature using MGSE monitors the flow or diffusion of single components, often water in a porous bed.[21,71] As long as there is just one component contributing to the signal the chemical shift is redundant. However, when examining systems containing water, oil and/or surfactant, such as emulsions and liquid crystals, all components behave differently and contribute to the signal in different ways. In these cases chemical shift resolution could be crucial to determine the characteristics of the material properly. By monitoring the different components one can determine which are restricted or obstructed which is invaluable in trying to determine the phase of a sample. Having these reasons in mind we set out to modify existing MGSE-sequences to be able to obtain

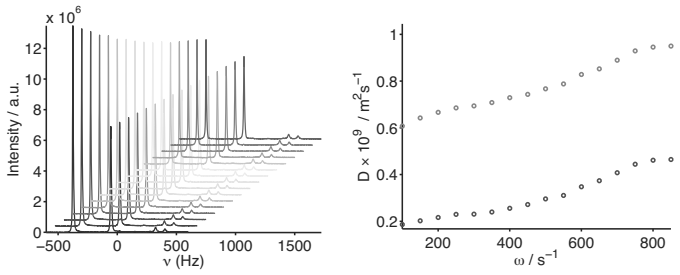

Figure 5.2: To the left is the spectrum for the vesicle gel used in paper IV for $T_m = 10$ ms. In the spectrum the big peak to the left originates from water and the two right peaks come from the oil and surfactant tails, while the origins of the middle peak is the counterion TMA. As the gradient or b values increase the spectrum color goes from blue to red. To the right is the experimental diffusion spectrum for water (red) and TMA (blue) also for the vesicle gels. The oil peaks has been omitted from the diffusion spectrum because of their low diffusivity and signal intensity.

chemical shift resolution.

The sequence was first tried out on a concentrated emulsion to be able to verify the method by comparing with previous results, paper III. The next step was to use it in other samples and it was then combined with measurements of λ_{hom} in paper IV. Both the applied techniques in this paper indicated structural features which had not be observed before. Combining the previous and new results a more complex structure could be proposed.

5.3 Measuring Yeast Cell Properties

Sedimented yeast cell suspensions were used as model systems to examine the methods presented in papers VI and V. By using ordinary PGSE-experiments in two different ways, D_0 for the intracellular water and the cellmembrane permeability could be measured.

The troublesome part of using PGSE on restricted diffusion is that the time parameters, δ and t_d, become very important for how the echo decay behaves. Earlier efforts on this subject have been focusing on obtaining size information from an echo decay for limiting cases of equation 4.13, generally geometry and/or time parameters.[12,13,36] In paper V we present equation 4.13 which is valid independently of the choice of time parameters or geometry. By combining this equation with a bi-

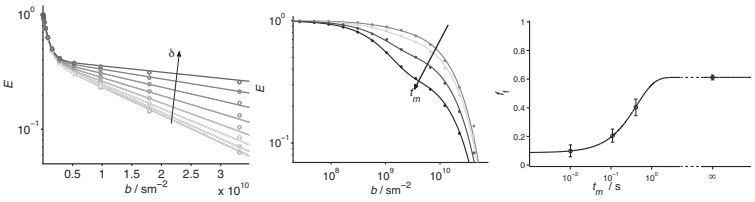

Figure 5.3: To the left is a graph of the echo decays as δ is varied from 0.5 to 20 ms indicated with different colors. From this data and using equation 4.13 the intracellular diffusion coefficient can be obtained. In the middle is a graph over the echo decays from a FEXSY-experiment using t_m of 10.1 (red), 109.1 (green) and 409.1 (blue) ms and appropriate to obtain f_f^{eq} (black). To the right the fitting of equation 4.25 for the data shown in the middle. The errorbars in the markers indicate one standard deviation for the fitting obtained using Monte Carlo error estimation.[72] All the data presented were obtained for a sedimented yeast cell suspension at 20°. Further experimental details can be obtained in papers V and VI.

exponential decay the intracellular diffusion coefficient for a yeast cell suspension could be determined. The intracellular diffusion is an important parameter to get insight on the intracellular space and the objects present there in but is not trivial to measure because of the surrounding cell wall.

There has mainly been two technical basis to measure cell water exchange or permeability using diffusion NMR. One of them uses a model based on first order kinetics (known as the Kärger model) to analyze the measured echo decays.[55] The other combines two PGSE for which g is varied independently of each other (known as DEXSY) and the obtained signal is then put through a 2D inverse Laplace-transformation.[56] The former has the advantage that the obtaining one or a couple of echo decays can be done within minutes and by fitting the decays to the model an exchange time can be obtained. The drawback is that the equations used are generally limited to certain cases and the fitting needs knowledge of the system to be appropriate. The latter has the advantage that after the inverse Laplace-transformation of the 2D dataset has been done an appearance of cross-peaks directly indicate the presence of exchange. However, a 2D inverse Laplace-transform requires a large dataset to be reliable[57] and thus a long experimental time is needed. In paper VI we take the advantage of the fitting for the former technique but also take the advantage of the direct way of identifying an exchange for the latter technique. This is done by reducing the number of dimensions in

the DEXSY-experiment and combining it with equations similar to the Kärger model. In this way the cell permeability and exchange time can be obtained to a good certainty in less than quarter of an hour.

5.4 Interbilayer Forces

For this project centrifugation, to obtain gravitational forces, and chemical shift imaging, to measure concentration, were combined to calculate interbilayer forces, i.e. the interaction between bilayers. The results for the relatively simple method (from an experimental point of view) are presented in paper VII.

Interbilayer forces are important for the stability of a lamellar system but is not always straight forward to obtain.[73] Scattering techniques and surface force measurements could work but is limited to the type of samples for which it is possible. Using centrifugation one obtains an equilibrium between internal and centrifugal forces. The centrifugal forces are set by the centrifugation settings while the internal forces are monitored through a concentration profile.[74] The trick here is thus to choose what technique to use to obtain the concentration profile. Since equilibrium is required a technique for which the sample can be monitored non-destructively is desired to be able to compare different centrifugal times to be certain of that equilibrium is really reached. For this purpose magnetic resonance with chemical shift resolution is ideal, it is non-destructive implicating that the sample can be measured on and then put back in the centrifuge and using chemical shift resolution the concentration can easily be determined.

We tried the new combination on a lamellar phase containing D_2O. The quadrupolar splitting from the deuterium is a good marker for concentration and the internal forces consist of only interbilayer interactions. Independently of whether the calculations were done using the free energy or the osmotic pressure the bending rigidity was determined to $\approx$5 kT which should be a verification of that the method is appropriate. Important to note is that an ordinary table-top centrifuge, which should be common in any chemical lab, and an NMR with gradient possibilities, which is also quite common, makes it possible to measure interbilayer forces.

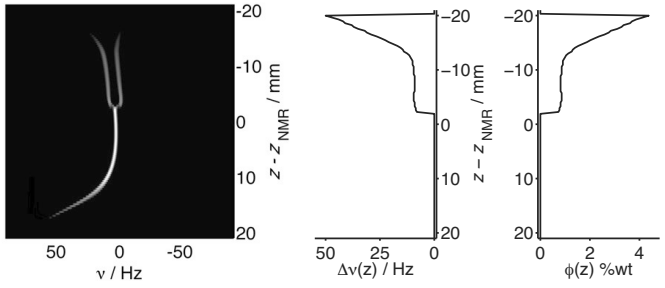

Figure 5.4: The NMR data for an inhomogeneous sample of 2.7wt% C_10E_3 in a mixture of H_2O and D_2O (0.25wt% and 99.75%, respectively) after centrifugation for 21 days. To the left is a 2D correlation spectrum with resonance frequency on the x-axis and position on the y-axis, in the middle is a graph of how the quadrupolar splitting changes with position and to the right is a graph of how the concentration of surfactant changes with position. The position is noted as $z - z_{\mathrm{NMR}}$ where z is the position in the centrifugal field and z_{NMR} is the isocenter of the NMR-spectrometer.

Chapter 6

Conclusions/Outlook

In this work a series of new methods using gradient NMR has been introduced and verified on different types of soft materials. One should mention them as methods because nothing is new from a fundamental and experimental NMR point-of-view but they are rather new ways of using the existing sequences or analyzing the obtained results. To determine λ_{hom} or D_0 for intracellular water ordinary PGSE- and PGSTE-sequences are used, which have been around since the late 60:s. By a set of experiments where the gradient pulse duration is changed systematically these parameters can be determined. The idea of the MGSE-experiment was introduced in the beginning of the 80:s but there has not been any real concern about the chemical shift resolution. The DEXSY-sequence is about 10 years old, by changing which dimensions are important (and thus making it into a FEXSY-experiment) a different type of information can be obtained in a more analytical way. Centrifugation has been used as an analytical tool for almost 100 years and is here combined with the more than 25 year old CSI to obtain a concentration profile in a non-invasive way. This means that an ordinary centrifuge and an ordinary NMR-spectrometer with gradient possibility is all that is needed to measure the interbilayer forces.

Since none of the methods needs any "state-of-the-art" equipment they should all have potential to become standard evaluation methods for determining material properties. This would include both industrial (to examine the product) and medical (as a diagnostic tool) applications, even if some further evaluation and development is probably needed. These advances could include combining the method imaging to get spatial resolution, work on possibilities to decrease the signal-to-noise dependence or using them on other systems and examine if reasonable results are obtained for them as well.[75]

Populärvetenskaplig sammanfattning på svenska

Kärnmagnetresonans (NMR) har en stor fördel som teknik för att mäta materialegenskaper då det är en icke-destruktiv metod. Med andra ord är det man mäter på likadant före som efter mätningen är gjord. Detta medför att det blivit intressant som en diagnostiseringsteknik inom sjukvården där begreppet magnetkamera används som namn för tekniken.

I detta arbete har nya metoder för att undersöka olika materialegenskaper med hjälp av NMR för diffusion och avbildning utvecklats. I båda dessa fall används tillfälliga gradienter i magnetfältet som gör att kärnornas position kan identifieras. Vid avbildning används gradientpulsen för att bestämma molekylpositionerna och man får en koncentrationsbild. Molekylernas förflyttning är det som mäts vid diffusionsmätningar.

Ett materials homogena längdskala är ett mått på storleken på den struktur som finns i materialet. Undersöker man materialet på kortare längder så kommer man att uppfatta förekomsten av en struktur men ser man på större längder kommer strukturen att försvinna och det kommer att se ut som ett homogent material. Ett av projekten i detta avhandlings-arbete var att utveckla en metod för att mäta den homogena längdskalan.

Att kunna identifiera förflyttningen av flera olika sorters molekyler gör att man kan observera hur hinder och restriktioner påverkar olika molekyler på olika sätt. Denna information kan i sin tur säga något om restriktionernas egenskaper. Genom att modifiera en befintlig teknik var det möjligt att få ytterligare information om materialet.

Bagerijäst användes som modellsystem för att utvärdera två olika metoder där den ena mäter intracellulär diffusion och den andra membranpermeabilitetet. Båda dessa egenskaper kan vara till hjälp vid sjukdomsdiagnostisering inom sjukvården.

Genom att mäta koncentrationsprofiler för olika prover som centri-

fugerats tills dess att jämvikt uppnåtts kan man betsämma böjningsstelheten hos bilager. Denna egenskap inkluderar information om bilagrets och därmed den lamellära fasens stabilitet.

Det har verifierats att alla de nya metoderna fungerar och ger rimliga resultat. Med ytterligare utvärderingar bör de ha potential till att bli standardmetoder för att mäta materialegenskaper.

References

[1] Agre, P. *Angew. Chem. Int. Ed.* **2004**, *43*, 4278–4290.

[2] Hamley, I. W. *Introduction to Soft Matter: Polymers, Colloids, Amphiphiles and Liquid Crystals*; John Wiley & Sons Ltd, Chichester, 2000.

[3] Evans, D. F.; Wennerström, H. *The Colloidal Domain: where Physics, Chemistry and Technology Meet*, 2nd ed.; Advances in Interfacial Engineering Series; Wiley - VCH, New York, 1999.

[4] Holmberg, K.; Jönsson, B.; Kronberg, B.; Lindman, B. *Surfactants and Polymers in Aqueous Solution*, 2nd ed.; John Wiley & Sons Ltd, Chichester, 2003.

[5] Wennerström, H.; Olsson, U. *C. R. Chimie* **2009**, *12*, 4–17.

[6] Regev, O.; Backov, R.; Faure, C. *Chem. Mater.* **2004**, *16*, 5280–5285.

[7] Attard, G. S.; Glyde, J. C.; Göltner, C. G. *Nature* **1995**, *378*, 336–368.

[8] Spowart, J. E.; Maruyama, B.; Miracle, D. B. *Mater. Sci. Eng.* **2001**, *A307*, 51–66.

[9] Campbell, N. A.; Reece, J. B.; Mitchell, L. G. *Biology*, 5th ed.; Benjamin/Cummings, Menlo Park, 1999.

[10] Grebenkov, D. S. *Concepts Magn. Reson. A* **2010**, *36A*, 24–35.

[11] Kärger, J.; Heink, W. *J. Magn. Reson.* **1983**, *21*, 1–7.

[12] Murday, J. S.; Cotts, R. M. *J. Chem. Phys.* **1968**, *48*, 4938–4945.

[13] Neuman, C. H. *J. Chem. Phys.* **1974**, *60*, 4508–4511.

[14] Nordin, M.; Jacobi, M. N.; Nydén, M. *J. Magn. Reson.* **2009**, *201*, 205–211.

[15] Mitra, P. P.; Sen, P. N.; Schwartz, L.; LeDoussal, P. *Phys. Rev. Lett.* **1992**, *68*, 3555–3558.

[16] Price, W. S.; Barzykin, A. V.; Hayamizu, K.; Tachiya, M. *Biophys. J.* **1998**, *74*, 2259–2271.

[17] Robertsson, B. *Phys. Rev.* **1966**, *151*, 273–277.

[18] Stepišnik, J. *Prog. Nucl. Magn. Reson. Spectrosc.* **1985**, *17*, 187–209.

[19] Callaghan, P. T.; Stepišnik, J. *J. Magn. Reson. A* **1995**, *117*, 118–122.

[20] Stepišnik, J. *Physica B* **1993**, *183*, 343–350.

[21] Stepišnik, J.; Lasič, S.; Mohoric, A.; Sersa, I.; Sepe, A. *J. Magn. Reson.* **2006**, *182*, 195–199.

[22] Hore, P. J. *Nuclear Magnetic Resonance*; Oxford Chemistry Primers; Oxford University Press, 1995.

[23] Levitt, M. H. *Spin Dynamics: Basics of Nuclear Magnetic Resonance*, 2nd ed.; John Wiley & Sons Ltd, Chichester, 2008.

[24] Hahn, E. L. *Phys. Rev.* **1950**, *80*, 580–594.

[25] Pake, G. E.; Purcell, E. M. *Phys. Rev.* **1948**, *74*, 1184–1188.

[26] Halle, B.; Wennerström, H. *J. Chem. Phys.* **1981**, *75*, 1928–1943.

[27] Callaghan, P. T. *Principles of Nuclear Magnetic Resonance Microscopy*; Oxford University Press, 1991.

[28] Price, W. S. *NMR Studies of Translational Motion*; Cambridge University Press, 2009.

[29] Bar-shir, A.; Avram, L.; Özarslan, E.; Basser, P. J.; Cohen, Y. *J. Magn. Reson.* **2008**, *194*, 230–236.

[30] Balinov, B.; Jönsson, B.; Linse, P.; Söderman, O. *J. Magn. Reson. A* **1993**, *104*, 17–25.

[31] Malmborg, C.; Sjöbeck, M.; Brockstedt, S.; Englund, E.; Söderman, O.; Topgaard, D. *J. Magn. Reson.* **2006**, *180*, 280–285.

[32] Malmborg, C.; Topgaard, D.; Söderman, O. *J. Magn. Reson.* **2004**, *169*, 85–91.

[33] Linse, P.; Söderman, O. *J. Magn. Reson. A* **1995**, *116*, 77–86.

[34] Blees, M. H. *J. Magn. Reson. A* **1994**, *109*, 203–209.

[35] Caprihan, A.; Wang, L. Z.; Fukushima, E. *J. Magn. Reson. A* **1996**, *118*, 94–102.

[36] Mitra, P. P.; Halperin, B. I. *J. Magn. Reson. A* **1995**, *113*, 94–101.

[37] Stejskal, E. O.; Tanner, T. J. *J. Chem. Phys.* **1965**, *42*, 288–292.

[38] Tanner, J. E. *J. Chem. Phys.* **1970**, *52*, 2523–2526.

[39] Wu, D.; Chen, A.; Charles S. Johnson, J. *J. Magn. Reson. A* **1995**, *115*, 260–264.

[40] Callaghan, P. T.; Eccles, C. D.; Xia, Y. *J. Phys. E* **1988**, *21*, 820–822.

[41] Barzykin, A. V. *J. Magn. Reson.* **1999**, *139*, 342–353.

[42] Bergman, D. J.; Dunn, K.-J.; Schwartz, L.; Mitra, P. P. *Phys. Rev. E* **1995**, *51*, 3393–3400.

[43] Callaghan, P. T. *J. Magn. Reson. A* **1995**, *113*, 53–59.

[44] Callaghan, P. T. *J. Magn. Reson.* **1997**, *129*, 74–78.

[45] Codd, S. L.; Callaghan, P. T. *J. Magn. Reson.* **1999**, *137*, 358–372.

[46] Grebenkov, D. S. *J. Chem. Phys.* **2008**, *128*, 134702.

[47] Yadav, N. N.; Price, W. S. *J. Colloid Interface Sci.* **2009**, *338*, 163–168.

[48] Callaghan, P. T.; Coy, A.; MacGowan, D.; Packer, K. J.; Zelaya, F. O. *Nature* **1991**, *351*, 467–469.

[49] Callaghan, P. T.; Coy, A.; Halpin, T. P. J.; MacGowan, D.; Packer, K. J.; Zelaya, F. O. *J. Chem. Phys.* **1992**, *97*, 651–662.

[50] Coy, A.; Callaghan, P. T. *J. Colloid Interface Sci.* **1994**, *168*, 373–379.

[51] Lennon, A. J.; Kuchel, P. W. *J. Magn. Reson. A* **1994**, *111*, 208–211.

[52] Balinov, B.; Söderman, O.; Ravey, J. C. *J. Phys. Chem.* **1994**, *98*, 393–395.

[53] Kuntz, J.-F.; Palmas, P.; Canet, D. *J. Magn. Reson.* **2007**, *188*, 322–329.

[54] Stepišnik, J. *Physica B* **1999**, *270*, 110–117.

[55] Kärger, J. *Adv. Colloid Interface Sci.* **1985**, *23*, 129–148.

[56] Callaghan, P. T.; Furó, I. *J. Chem. Phys.* **2004**, *120*, 4032–4038.

[57] Song, Y.-Q.; Venkataramanan, L.; Hürlimann, M. D.; Flaum, M.; Frulla, P.; Straley, C. *J. Magn. Reson.* **2002**, *154*, 261–268.

[58] Mansfield, P.; Grannell, P. K. *Phys. Rev. E* **1975**, *12*, 3618–3634.

[59] Lauterbur, P. C. *Nature* **1973**, *242*, 190–191.

[60] Brown, T. R.; Kincaid, B. M.; Ugurbil, K. *Proc. Natl. Acad. Sci. USA* **1982**, *79*, 3523–3526.

[61] Harel, E.; Pines, A. *J. Magn. Reson.* **2008**, *193*, 199–206.

[62] Lafitte, G.; Thuresson, K.; Söderman, O. *J. Pharm. Sci.* **2006**, *96*, 258–263.

[63] Salvati, A.; Lynch, I.; Malmborg, C.; Topgaard, D. *J. Colloid Interface Sci.* **2007**, *308*, 542–550.

[64] Östlund, Å.; Bernin, D.; Nordstierna, L.; Nydén, M. *J. Colloid Interface Sci.* **2010**, *344*, 238–240.

[65] Labadie, C.; Lee, J.-H.; Vétek, G.; Springer, C. S. *J. Magn. Reson. B* **1994**, *105*, 99–112.

[66] Basser, P. J.; Mattiello, J.; LeBihan, D. *Biophys. J.* **1994**, *66*, 259–267.

[67] Chaumette, H.; Grandclaude, D.; Canet, D. *J. Magn. Reson.* **2003**, *163*, 369–373.

[68] Djemai, A.; Sinka, I. C. *Int. J. Pharm.* **2006**, *319*, 55–62.

[69] Coy, A.; Callaghan, P. T. *J. Chem. Phys.* **1994**, *101*, 4599–4609.

[70] Håkansson, B.; Pons, R.; Söderman, O. *Langmuir* **1999**, *15*, 988–991.

[71] Callaghan, P. T.; Codd, S. L. *Phys. Fluids* **2001**, *13*, 421–427.

[72] Alper, J. S.; Gelb, R. I. *J. Phys. Chem.* **1990**, *94*, 4747–4751.

[73] Bagger-Jörgensen, H.; Olsson, U. *Langmuir* **1996**, *12*, 4057–4059.

[74] Pages, M. G.; Zemb, T.; Dubois, M.; Cölfen, H. *ChemPhysChem* **2008**, *9*, 882–890.

[75] Lasič, S.; Nilsson, M.; Lätt, J.; Ståhlberg, F.; Topgaard, D. Submitted to Magn Reson Med.